Quasi Self-Excited DFIG-Based Wind Energy Conversion System

Russell Akbari
Member, IEEE
Purdue School of Engineering and Technology, IUPUI
Indianapolis, IN 46202, USA
rakbari@purdue.edu

Afshin Izadian
Senior Member, IEEE
Purdue School of Engineering and Technology, IUPUI
Indianapolis, IN 46202, USA
aizadian@purdue.edu

Robert Weissbach
Senior Member, IEEE
Purdue School of Engineering and Technology, IUPUI
Indianapolis, IN 46202, USA
rweissba@iupui.edu

***Abstract*—This paper introduces a new configuration of the DFIG-based wind energy conversion system (WECS) employing only a reduced-size Rotor Side Converter (RSC) in tandem with a supercapacitor. In the proposed structure, the Grid Side Converter (GSC) utilized in conventional DFIG-based WECSs is successfully eliminated. This is accomplished by employing the hydraulic transmission system (HTS) as a continuously variable and shaft decoupling transmission unit. This transforms the conventional constant-ratio drives by providing an opportunity to control the power flow through the generator's rotor circuit regardless of the wind turbine's shaft speed. This feature of HTS can be utilized to control the RSC power and ultimately regulate the supercapacitor voltage without a need for GSC. The proposed system is investigated and simulated in MATLAB Simulink at various wind speeds to validate the results and demonstrate the dynamic performance of the system.**

***Index Terms*—Reduced-size converters, doubly-fed induction generator (DFIG), hydraulic power transmission system, wind turbines, reactive power control.**

I. Introduction

Wind energy is a renewable, widely distributed, abundant, pollution-free resource and it has been expected to be developed as a significant energy source in the future [1, 2]. Recently, a global trend to install high-scale wind turbines has been increasing to make wind energy more cost-effective. Nevertheless, the cost of Wind Energy Conversion Systems (WECSs) should be decreased even more to compete globally with other sources of energy [3]. Currently, The Levelized Cost of Energy (LCOE) for offshore WECSs is remarkably higher than that of conventional fossil-fuel energy and most of the renewable resources such as hydropower, PV, and bioenergy [4].

The conventional gearbox drivetrain employed in WECSs, to drive either a Doubly-Fed Induction Generator (DFIG) or Permanent Magnet Synchronous Generator (PMSG), is one crucial, expensive, and heavy element in a conventional WECS and its failure is a major contributor to downtime and high maintenance cost of wind turbines [5-8]. Previous studies indicate that gearboxes normally do not attain their design lifetime and suffer from premature failures [5], and it is necessary to replace them every 5-7 years [9, 10]. Moreover, since all subassemblies are located in the nacelle in conventional WECSs, their installation and maintenance costs become large [11]. Furthermore, the structure of these wind turbines must be strong enough to withstand the heavyweight of the nacelle on top of the tower. Direct-drive wind turbines could ameliorate the reliability and efficiency of WECSs by eliminating the gearbox. However, this drive train is much heavier and more expensive than gearbox-based units [12, 13].

Alternatively, hydraulic technology can be a suitable solution to overcome the challenges of the traditional method of harvesting power from wind turbines. For instance, [14] shows that the weight of the nacelle could be decreased by 33-50% simply by relocating the generator and other subassemblies to the ground level. Then, by using an analytical technique and investigating natural frequencies of the tower for a 5-MW hydraulic wind powertrain, the weight of the tower itself compared with the conventional wind turbine can be cut to 50%, and the capital cost of the wind energy reduced by 4%. The result of [15] demonstrates the reduction of 35.5% in mass of the nacelle due to employing a hydraulic drivetrain and an average installed cost saving of 5.36-24.0% can occur for offshore wind. Despite the lower efficiency of HTS, which is about 85-88% [16, 17], the HTS could reduce the overall cost of the system and lower the Levelized Cost of Energy (LCOE) by 3.92-18.8% [15], and improve the Capacity Factor (CF) of the wind turbine [18]. Given a tower structure, the rotor speed of a wind turbine with HTS could be restricted at a higher speed that results in harvesting about 17% more energy and can compensate for its losses [19].

A wind turbine powertrain that relies on hydraulic machinery could provide a decoupled transmission system. Many studies have been conducted on different HTSs and use this property to employ a conventional synchronous generator (SG) and eliminate the power converters [20-30]. In these studies, two strategies are applied to maintain the SG at synchronous speed with a small allowed variation and subsequently control the frequency: first, relying on the damping factor of the SG [20-23], and second, inserting an energy buffer between the wind turbine and SG [24-29]. The former strategies can further reduce the efficiency of the synchronous generator due to the ever-changing nature of wind speed, and the latter necessitates the application of other extra subassemblies. Moreover, none of this research considers the dynamics of the synchronous generator. In [30] the authors consider the dynamical model of the SG and use the control

This is the author's manuscript of the article published in final edited form as:

Akbari, R., Izadian, A., & Weissbach, R. S. (2021). Quasi Self-Excited DFIG-Based Wind Energy Conversion System. IEEE Transactions on Industry Applications, 57(3), 2816–2824. https://doi.org/10.1109/TIA.2021.3067621

input to maintain the SG speed constant. However, the optimal aerodynamic operation of the system is not considered.

Unlike an SG in which the mechanical swing is defined by its primary mover power and damping factors, the speed of Doubly-Fed Induction Generators (DFIGs) can be controlled actively and its active and reactive powers can be controlled in a decoupled manner [31-33]. However, DFIG needs two power converters with a size of about 25-30% of the generator's rated power [34, 35]. To overcome the challenges which utilizing SG can bring about and to reduce the size of the Rotor Side Converter (RSC), this paper introduces a new reconfiguration for the hydraulic wind turbine. Moreover, since in the proposed configuration the Grid Side Converter (GSC) is eliminated, it is named the quasi self-excited DFIG-based WECS. The contributions of the paper are as follows:

- It is shown that compared with a conventional induction generator (IG), the proposed configuration provides full control over the reactive power of the wind turbine through the RSC alone.
- The paper introduces the capability of controlling the charge and discharge of the storage solely through the RSC.
- The size of the supporting power equipment to make a DFIG fully functional is drastically reduced.

This paper is structured as follows: the HTS and the Maximum Power Point Tracking (MPPT) approach are described in detail in section II. In section III the proposed configuration and its active and reactive power control method are elaborated. The design nuances of the proposed method are explained in section IV; and finally, simulation results are presented in section V.

II. Hydraulic Drivetrain

The configuration of the hydraulic-driven WECS is shown in Fig. 1. The hydraulic transmission system utilizes, a hydraulic pump and motor which transfers power through a pressurized fluid line. The high transmission ratio needed can easily be achieved by changing the displacement ratio of the pump and motor. Therefore, a variable-displacement pump or motor (or both) is needed to achieve the continuously variable transmission (CVT). Various hydraulic transmission systems have been investigated in the literature [36]. Herein, an HTS with a variable-displacement pump is considered since it is the simpler solution from the controllability perspective [37].

This configuration has a variable-displacement pump housed in the nacelle that is driven by the turbine shaft and a hydraulic motor located at ground level. As the wind speed increases, the hydraulic pump causes the pressure to increase at the inlet, and consequently, the motor produces more torque that drives the generator. At some point, when the driving and resisting torques are balanced, the pump and generator reach a steady angular speed of rotation.

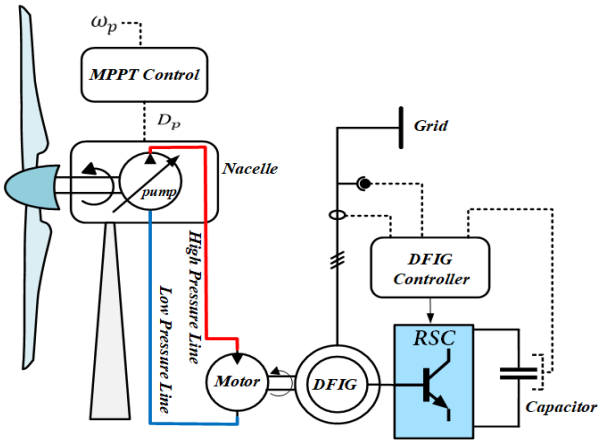

Fig. 1. Configuration of the hydraulic wind turbine and the generator controller.

A. Hydraulic Transmission System Model.

The hydraulic pump sustains several torques as it starts to rotate. The governing equations of the hydraulic pump that illustrates the flow and torque balance are as follows [38]:

$$Q_p = D_p\omega_p - K_{ps}\,P \tag{1}$$

$$J_r\frac{d\omega_p}{dt} = \tau_r - C_{vp}D_p\,\omega_p - C_{fp}\,D_pP - \tau_{bp} - D_p\,P \tag{2}$$

The pressurized flow reaching the hydraulic motor makes it start to rotate. The relation of the motor's displacement, its angular velocity, and the instantaneous flow rate is as follows:

$$Q_m = D_m\omega_m - K_{ms}P \tag{3}$$

$$J_m\frac{d\omega_m}{dt} = D_mP - C_{vm}D_m\omega_m - C_{fm}D_mP - \tau_{bm} - \tau_L \tag{4}$$

$$\frac{dP}{dt} = \left(\frac{\beta}{V}\right)(Q_p - Q_m) \tag{5}$$

The operating pressure dynamic follows the laws of fluid compressibility. Based on the principles of mass conservation and the definition of bulk modulus, the fluid compressibility within the system boundaries can be written as (5). The pressure losses of the lines are considered negligible.

B. Optimal Pump Displacement Control (OPDC)

Optimal power production of a wind turbine is achieved by optimizing the drivetrain to the important points of operation and simultaneous use of control strategies to ensure operation in those points. To obtain the maximum harvested power from the wind, the tip speed ratio must be optimum (λ_{opt}). Therefore, for different wind speeds, the pump speed is controlled through the pump displacement to obtain the maximum power coefficient (Cp_{max}). The optimum pump displacement is obtained as follows [39]:

$$D_{p-opt} = \left(\frac{1}{2\lambda_{opt}^3\,P}\right)\eta_m\rho_{air}\pi R^5\,Cp_{max}\omega_p^2 \tag{6}$$

In this WECS, the wind turbine angular velocity and the generator speed are decoupled by a hydrostatic power transmission system. dP/dt in (5) becomes zero in steady-state, and neglecting the losses, the speed turn ratio of the

hydraulic transmission is obtained as $\omega_m/\omega_p = \mathrm{D_p}/\mathrm{D}_m$. By changing the displacement of the pump, the hydraulic drivetrain behaves as a Continuously Variable Transmission (CVT) and could provide decoupled transmission of power.

III. The Proposed Configuration

A. Concept

The DFIG is a three-phase wound-rotor induction generator where the stator windings are directly connected to the electrical grid and its rotor windings are indirectly supplied through a back-to-back converter consisting of the RSC and GSC, connected through a DC link. The RSC is responsible for controlling the DFIG, while the GSC regulates the DC-link voltage. It is proven that the power passed through the DFIG's RSC is proportional to the generator slip [33, 34]. Moreover, in conventional gearbox-driven DFIG-based WECSs, the DFIG shaft is mechanically coupled to the wind turbine shaft, and its speed must be controlled proportionally to the wind speed to maintain the tip speed ratio close to the optimal tip speed ratio. As a result, to obtain MPPT, the generator's optimal speed must be controlled within a wide range of $\pm 30\%$, and the converters' power rating must be chosen accordingly.

On the other hand, the hydraulic drivetrain can provide an extra degree of freedom to control the generator speed by decoupling the shaft of the wind turbine and the generator shaft. By controlling the generator speed, the power flowing through the RSC can be independently controlled irrespective of the wind speed and turbine angular velocity [39]. Consequently, the GSC can be eliminated, and the rotor terminals can be supplied by only the RSC in conjunction with a capacitor as shown in Fig. 1. In this configuration, the rotor side converter should only process the losses of the system since the net power at the DC-link terminal should be zero; otherwise, the DC-link voltage will not be stable. Since this amount of power constitutes only a small portion of the system power rating, the power rating of the converter, which is only RSC, reduces noticeably.

B. Active Power Control

The DFIG flux equations in the stator-flux orientated (SFO) frame are as follows:

$$\lambda_{qs} = L_s i_{qs} + L_m i_{qr} = 0 \qquad \lambda_{ds} = L_s i_{ds} + L_m i_{dr} = L_m i_{m0} \tag{7}$$

$$\lambda_{qr} = \sigma L_r i_{qr} \qquad \lambda_{dr} = \sigma L_r i_{dr} + L_0 i_{m0} \tag{8}$$

where $\sigma = 1 - \frac{L_m^2}{L_r L_s}$, and $L_0 = \frac{L_m^2}{L_s}$. The steady-state voltage of the rotor and stator are calculated as follows:

$$V_{qs} = R_s i_{qs} + \omega_s \lambda_{ds} \qquad V_{ds} = R_s i_{ds} \tag{9}$$

$$V_{qr} = R_r i_{qr} + s\omega_s \lambda_{dr} \qquad V_{dr} = R_r i_{dr} - s\omega_s \lambda_{qr} \tag{10}$$

The rotor power equation can be achieved as follow:

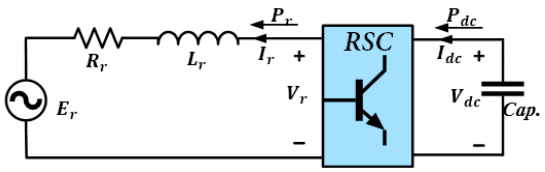

Fig. 2. Single-phase equivalent circuit of the DFIG rotor

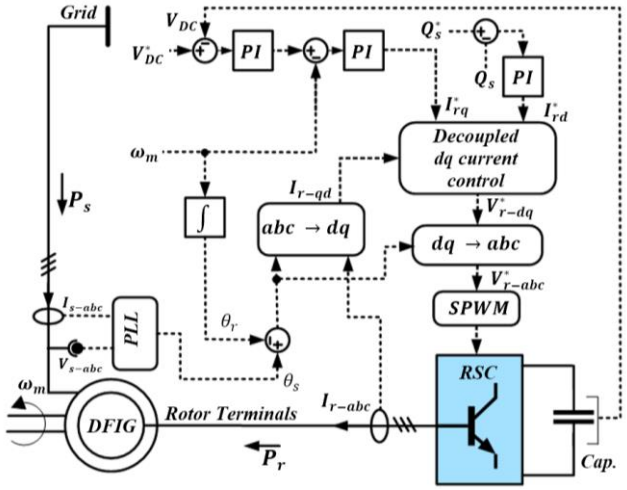

Fig. 3. (a) The active and reactive power control scheme of the proposed configuration.

$$P_r = \frac{3}{2} R_r \left(i_{qr}^2 + i_{dr}^2\right) + \frac{3}{2} s\omega_s L_0 i_{m0} i_{qr} = P_{lr} + P_{ar} \tag{11}$$

The calculated power P_r is the amount of power injected into the rotor windings at their terminals. The first term in (11) represents the rotor windings losses, P_{lr}, and the second term stands for the power transferred to the airgap, P_{ar}, which depends on the generator slip. The stator power, similarly, can be divided into two terms as follow:

$$P_s = \frac{3}{2} R_s \left(i_{qs}^2 + i_{ds}^2\right) + \frac{3}{2} \omega_s L_m i_{m0} i_{qs} = P_{ls} + P_{as} \tag{12}$$

where, P_{ls} and P_{as} are the stator windings losses and the stator-part airgap power respectively. From (7), (11), and (12), the relation between P_{as} and P_{ar} can be deduced as follows:

$$P_{ar} = -sP_{as}. \tag{13}$$

The airgap power comprises P_{as} and P_{ar}. The single-phase equivalent circuit of the generator rotor is shown in Fig. 2. The amount of power delivered by DC link, P_{dc}, is the sum of the P_r and the converter losses, P_{lc}, and can be written as follows:

$$P_{dc} = P_{lc} + P_{lr} - sP_{as} \tag{14}$$

In general, P_{dc}, must be zero to keep the DC-link voltage constant and provide an opportunity to eliminate the GSC. To this end, for any given power, the generator speed can be controlled such that equation (14) becomes zero. The control system in Fig. 3 demonstrates the same concept. The speed reference is determined by a proportional-integrator (PI) controller such that the DC-link voltage remains constant.

C. Reactive Power Control

Since in the proposed configuration the DFIG is only connected to the electrical grid through its stator, controlling

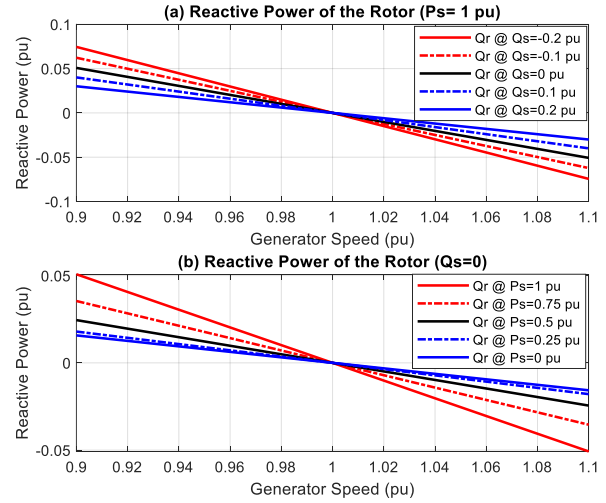

Fig. 4. (a) Rotor reactive power at $P_s = 1\ pu$ in various stator's reactive power (b) rotor reactive power at $Q_s = 0$ in various stator's active power

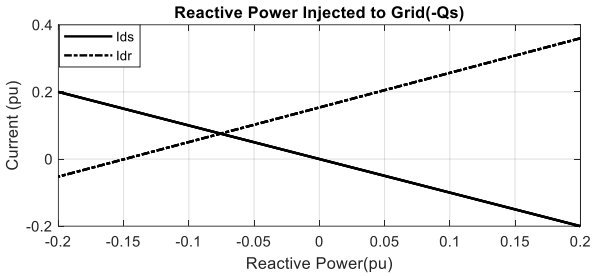

Fig. 5. Rotor and stator direct component of current in various stator reactive current

the stator reactive power is the only way to control the reactive power of the WECS. Reactive power control of DFIGs is well-known and easy and has been investigated extensively [31-34]. By using the feed-forward control loop to decouple the active and reactive power controls, the reactive power can be controlled by the direct component of the rotor current as shown in Fig. 3. The reactive power equations of DFIG can be expressed as follows:

$$Q_s = \frac{3}{2}\omega_s L_m i_{m0} i_{ds} \tag{15}$$

$$Q_r = s(Q_m - Q_s) + \frac{3}{2}s\omega_s \sigma L_r \left(i_{qr}^2 + i_{dr}^2\right) \tag{16}$$

where $Q_m = 1.5\omega_s L_0 i_{m0}^2$ is the magnetizing reactive power. Based on the amount of reactive power required at the stator, Q_s, the direct component of the stator current is identified; then using (7), the direct component of the rotor current can be identified. The only limitation, here, is the maximum current boundary of the rotor and stator winding. Fig. 4 (a) indicates the rotor reactive power for various stator reactive power at different generator speeds around the synchronous speed. To inject reactive power to the grid e.g. $Q_s = -0.2\ pu$, the rotor's reactive power follows a certain behavior depending on the generator's speed as shown in Fig 4. Since there is i_{qr} in the reactive power equation of the rotor (16), Fig. 4 (b) demonstrates the effects of changing the output active power on the reactive power of the rotor. However, in a given stator reactive power, the direct component of the rotor current remains the same no matter what the stator active power is. In other words, the direct component of the rotor current should be controlled to adjust the reactive power that the generator injects into the grid. Fig. 5 demonstrates the relationship between the reactive power of the generator and the direct component of the rotor and stator current, which is calculated based on (7) and (15). To inject the reactive power to the grid the direct component of the rotor current should be increased further to compensate for the magnetizing current of the generator.

IV. Design Considerations

In the steady-state, when P_{dc} becomes zero to keep the DC-link voltage constant, the targeted generator slip is small. In other words, the operating points are close to synchronous speed. This slip can be obtained by making equation (14) zero, which results in:

$$s_t = \frac{P_{lc} + P_{lr}}{P_{as}} \tag{17}$$

The numerator in (17) shows the rotor winding loss and converter loss. As the slip is small, these terms are small positive values. The denominator is negative when the electric machine operates in generator mode. Therefore, the targeted slip s_t is a small negative value. Its negative sign dictates that the generator must operate at a super synchronous speed. The relatively small slip implicitly indicates that the generator does not need a large voltage at the rotor side. For instance, if the rotor-side losses are only 2% of airgap power, which results in a slip of -2%; consequently, the rotor needs to be supplied with only about 2% of its nominal voltage. Since the losses of the rotor-side are relatively small for all operating points at different wind speeds, the DC-link voltage could be chosen as a small voltage.

Moreover, even during transients or in the presence of disturbances, the capacitor on its own must handle the rotor voltage. The larger the capacitor, the lower the effects of the disturbances on the DC-link voltage. In low-voltage DC-links, a supercapacitor becomes suitable. In conventional wind turbine the size of the capacitor is highly dependent on the bandwidth of current and dc-link voltage regulators. Commonly, the bandwidth of the current controller is chosen about 250-500 Hz and the bandwidth of the voltage regulator which is the second layer is chosen less than 100 Hz. Therefore, the capacitor of dc-link should be large enough to allow the GSC to maintains the dc-link voltage [40-43]. However, Since the dc-link regulator is the third layer of controller in the proposed configuration, its bandwidth is chosen 1/10 or 1/5 of the speed bandwidth and this controller should handle the dc-link voltage. Therefore, the amount of this capacitor is chosen such that:

$$C \geq \left(\frac{s_{max} P_n}{V_{dc}}\right) * \frac{5\tau_{vd}}{\Delta V_{dc}} \tag{18}$$

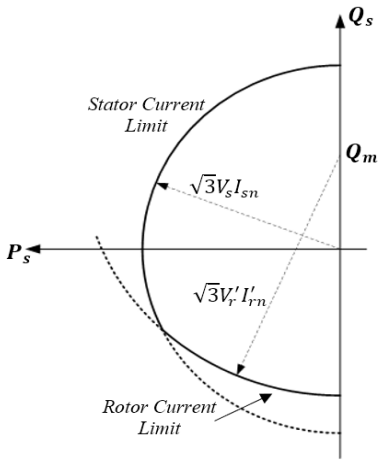

Fig. 6. Power capability curve of the generator

where, τ_{dc} is the time constant of the dc-link voltage regulator, and ΔV_{dc} is the maximum voltage variation on the dc link. s_{max} and P_n are the maximum slip and nominal power of the wind turbine.

Consequently, the switches are required to be sized according to the voltage and current rating. A suitable rotor to stator winding turns ratio could help to design the RSC and result in properly rated switches. The voltage and current rating of the DFIG rotor winding at the rotor side are obtained as follows [34]:

$$V_r' = nV_s \tag{19}$$

$$I_r' = \frac{S_n}{\sqrt{3}V_r'} = \frac{S_n}{\sqrt{3}nV_s} \tag{20}$$

where S_n is rated apparent power of the DFIG and n is the rotor to stator turns ratio of the generator. It is proven that the maximum voltage required for the rotor winding which is the rated voltage of the RSC is as follows [34]:

$$V_{con} = s_{max}V_r' = s_{max}nV_s \tag{21}$$

where s_{max} is the maximum of the absolute value of the generator slip. Since the slip is small, the amount of V_{con} is also small. Increasing n leads to an increase in V_{con} and a reduction in I_r'. With a fixed rotor winding copper volume, the rotor losses remain constant by increasing n. Therefore, it is beneficial to employ a DFIG with a large n. This value can be chosen based on the voltage and current rating of the power electronic switches.

To calculate the rotor apparent power two assumptions are made here. First, the leakage inductances of the generator are neglected ($\sigma = 0$), and second, the rotor loss is negligible. The active and reactive power of the DFIG rotor per unit is calculated as follow:

$$\begin{gathered} Q_{r-pu} = sI_{pu}^{dr}, \quad Q_s = I_{pu}^{ds}, \\ I_{pu}^{qs} = -I_{pu}^{qr} \ , \quad I_{pu}^{ds} = i_{m0-pu} - I_{pu}^{dr} \\ P_{r-pu} = -sP_{s-pu} \end{gathered} \tag{22}$$

Equation (22) shows that the maximum i_{dr} depends on the maximum capacitive reactive power. Therefore, the power

TABLE I. 1.5 MW WIND TURBINE DATA USED IN SIMULATION.

	Generator Data	
$\mathbf{P_s}$	Generator Power	1.5 MW
$\mathbf{V_s}$	Grid Voltage (line to line)	690 V
$\mathbf{L_{ls}/L_{lr}}$	Stator/Rotor Inductance	0.167/0.133 mH
$\mathbf{L_m}$	Magnetizing Inductance	5.48 mH
n	Stator to Rotor Winding Turn Ratio	15
$\mathbf{R_s}$	Stator Winding Resistance	2.65mΩ
$\mathbf{R_r'}$	Rotor Winding Resistance	2.63*15*15 mΩ
$\mathbf{I_{rn}'}$	Rated Current of Rotor	100 A
p	Generator pole pairs	2
C	Capacitance	20 F

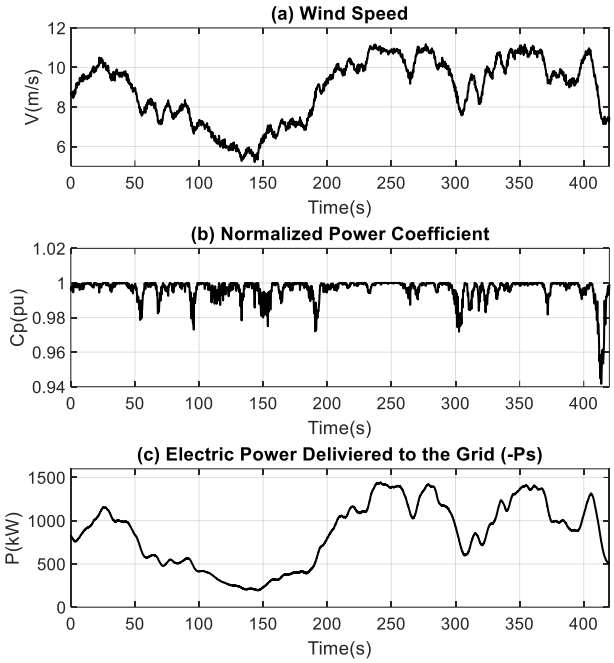

Fig. 7. (a) Wind speed (b) normalized power coefficient (c) electrical power delivered

rating of the RSC can be achieved as follows:

$$S_{pu}^r = s_{max}\sqrt{\left(Q_{m-pu} - Q_{s-pu}\right)^2 + P_{s-pu}^2} \tag{23}$$

RSC rating power depends on s_{max}, which is dependent on the rotor winding and power converter losses, and the maximum reactive power injected into the grid. The proposed configuration is capable of injecting or absorbing reactive power to/from the grid. Two main limitations of the generator power are stator and rotor limits. Using (22) and (23) the Power capability curve of the generator can be achieved as Fig. 6. Similar to SG's power capability curve, the maximum stator current limits the active and reactive power within a circle centered at the origin. However, the rotor current limit is a circle centered at (0, Q_m). This means, when Q_s is negative (inject reactive power to the grid) the rotor circuit should provide not only a magnetizing current but also an extra reactive term. In this case, similar to the conventional SG, the generator operates in overexcitation mode. When the magnetizing current partially or fully is supplied through the stator, the generator is operating in under-excitation mode.

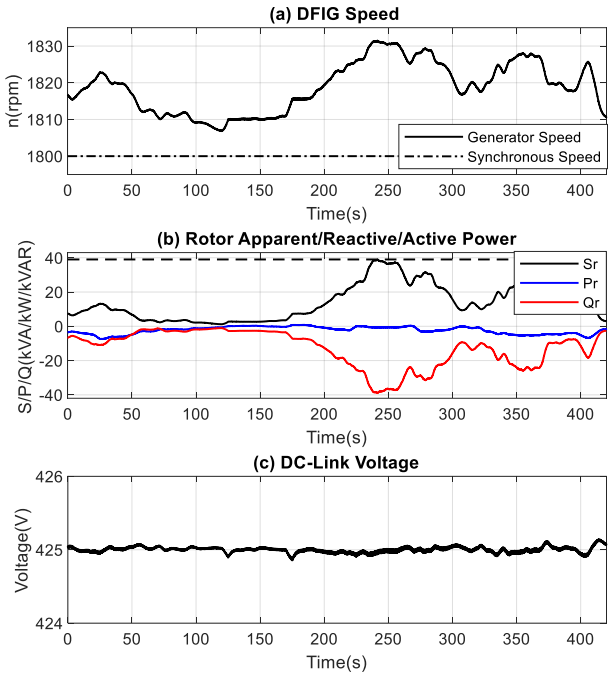

Fig. 8. (a) Rotor speed (b) rotor active and reactive power (c) capacitor voltage

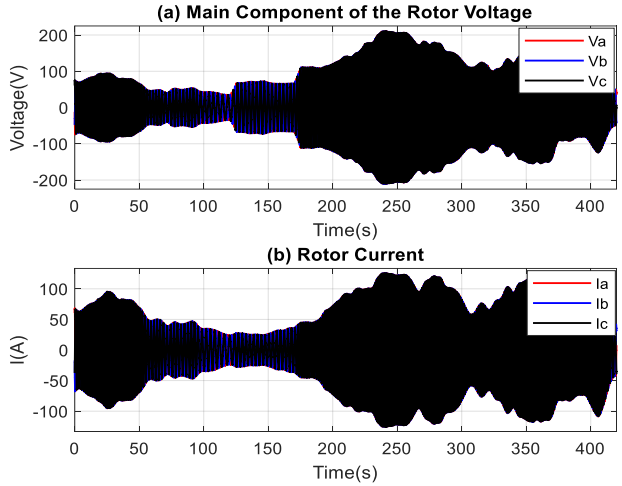

Fig. 9. (a) Main component of the rotor voltage (b) rotor current

V. Simulation and Discussion

A 1.5 MW wind turbine with HTS is modeled and sized for a case study. The wind turbine parameters are provided in Table I. The loss of the DFIG rotor can be calculated to be about 1.5 % where s_{max} is about 2.5%. Since the stator line voltage is 690 V, the rated rotor line voltage and rotor current at the turns ratio of $n = 15$ are calculated as 10350 V and 100 A, respectively. However, the maximum voltage required for the rotor, depending on the maximum slip percentage is, $10350 \times 0.025 = 259$ V. Therefore, the DC-link voltage required to establish the excitation voltage is $2\sqrt{2/3} \times 259 = 425$ V. From (23) and using data in Table I, the apparent power

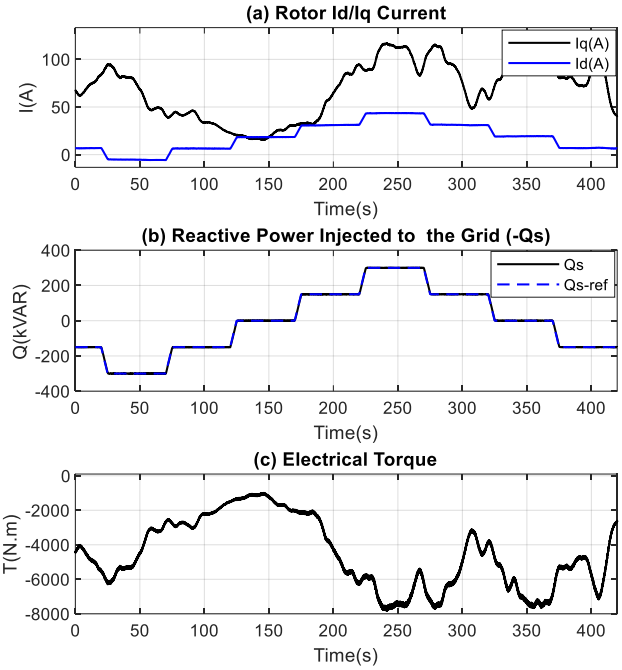

Fig. 10. (a) Rotor current (b) electrical torque

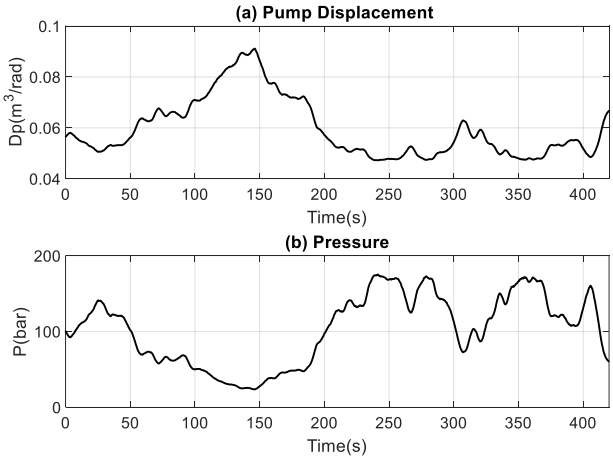

Fig. 11. (a) Pump displacement (b) pressure of the pipeline

rating of the power converter can be calculated to be 40 kVA. However, this is an estimation by considering a margin for DFIG slip. A system with more detail has resulted in a 2.7% (39 kVA) rating.

The wind speed is set to vary from 5 to 11 m/s as shown in Fig. 7.a. This wind speed profile and the maximum power point tracking utilized resulted in an MPPT tracking profile as shown in the normalized power coefficient in Fig. 7 (b). The MPPT control method was able to track maximum power points at various wind speeds, harvesting the maximum power from the existing energy in the wind. The actual output power reached a maximum of 1460 kW and a minimum of 200 kW as shown in Fig. 7 (c). However, the generator has been successfully controlled to track the maximum power of the wind. The control command in this case influences the generator's rotational speed. Fig. 8 (a) illustrates the generator

speed and the possibility of controlling the generator speed precisely in a small window above the 1800 rpm synchronous speed. This results in a -1.7% slip in the generation mode.

In this slip range, the rotor's active power is adjusted to provide the converter losses as shown in Fig. 8 (b). The reactive power of the rotor, which is proportional to the generator slip, is demonstrated in Fig. 8 (b). Since the maximum apparent power of the generator rotor happens when the maximum active power and the maximum reactive power injected into the gird coincide. This coincidence happens around 250s. As shown, the apparent power rating of the converter does not exceed 39 kVA maximum. Compared to conventional DFIG with two power converters at rating power of $2 \times 30\%$ of the generator's rated power (2×450 kVA), this configuration only requires one converter at about 2.7% of rated power, a maximum of 39 kVA. The DC-link voltage profile is shown in Fig. 8 (c). Since the amount of the generator slip is changing in a small range, the DC-link voltage required to inject the reactive power to the generator is smaller than that of the conventional DFIG. Therefore, the configuration is suitable for utilizing the supercapacitor at the rotor circuit. The capacitor is considered large enough (20 F) to reduce the variation of DC-link voltage during an extreme change of wind speed. This figure demonstrated that the DC-link controller was capable of maintaining the DC-link voltage and resulted in small variations of less than 0.2 V in extreme wind speed variations.

Accurate control over the slip of the generator resulted in a small fundamental component of the rotor voltage (Fig. 9 (a)). The small rotor voltage and the resulting DC-link voltage reduced the voltage stresses of the power electronic devices which lead to an increase in the reliability of the RSC and subsequently the whole system. Meanwhile, the smaller DC-link voltage led to smaller switching losses of the power electronic devices, and increased efficiency, and reduced the thermal stresses of the converter. Fig. 9 (b) shows the three-phase rotor currents which vary directly proportional to wind speeds. The direct and quadrature components of the rotor current are shown in Fig. 10 (a). The active power was controlled by controlling the generator torque (Fig. 10 (c)) or the quadratic current as i_{qr}. As shown, the torque and i_{qr} were proportionally varying with the wind speeds. The reactive power injected into the grid (Fig. 10 (b)) was controlled following the reference of i_{dr}. It was proven that the controller was effectively capable of controlling the active and reactive power of the system.

The drivetrain of the wind turbine also provided a unique dynamic in that the interface torque controller produced a command for the hydraulic pump displacement and as a result, the pressure of the system varied. Fig. 11 (a) demonstrates the displacement of the pump which was controlled to achieve the optimal aerodynamic power. The pressure of the pipeline shown in Fig. 11 (b) varied with the wind speed.

Table II compares the proposed configuration with a conventional gear-box driven DFIG in a 1.5 MW wind turbine. In conventional DFIG the slip of generator is chosen $\pm 30\%$. Therefore, the DC-link voltage should be chosen such that both GSC and RSC be able to operate properly ($V_{DC} \geq 2\sqrt{2/3}$*690=1100 V) [42]. However, this amount was calculated 425 V for the proposed configuration. This also indicated that the voltage stress of power electronic devices in the proposed configuration is much less. Current stress of semiconductor devices was obtained 1150 A for conventional DFIG compared to 125 A for the proposed configuration. Assuming the stator of the conventional DFIG operates at unity power factor, RSC should handle the maximum active power of the rotor and magnetizing current, and the GSC should also handle the portion of active power passed through rotor and the reactive power needed to inject to the grid. the

TABLE II. COMPAISION OF 1.5 MW CONVENTIONAL DFIG WITH THE POPOSED CONFIGURATION.

Parameter	Conventional DFIG	Proposed Configuration
$\mathbf{V_s}$	690 V	690 V
$\mathbf{P_s}$	1.5 MW	1.5 MW
n	1	15
$\mathbf{V_{DC}}$	1100 V	425 V
$\boldsymbol{I_{RSC}}$	1150 A	125 A
$\mathbf{S_{RSC}}$	412 kVA	40 kVA
$\mathbf{S_{GSC}}$	457 kVA	NA
C	20mF	20F

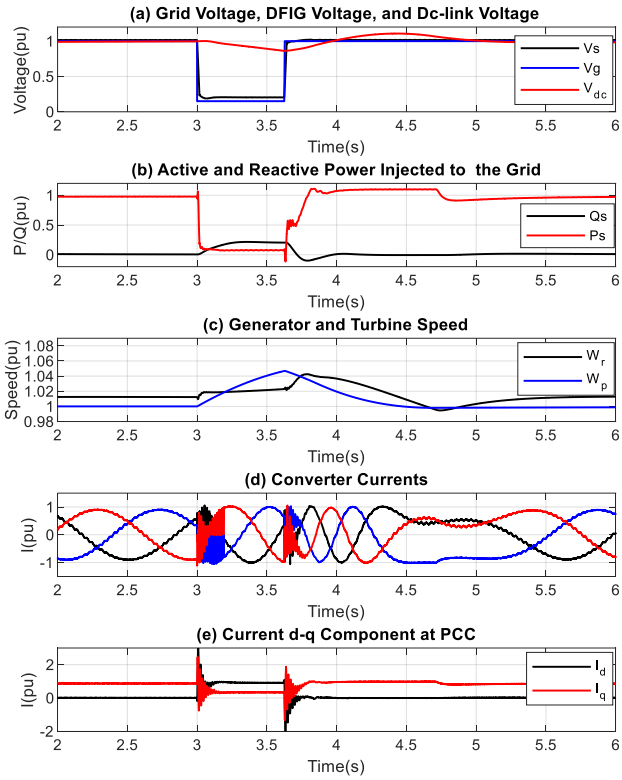

Fig. 12. LVRT analysis with voltage drop to 15% for 0.625 seconds (a) voltage at PCC, stator terminal, and dc link (b) active and reactive power injected to PCC (c) wind turbine and generator speed (d) converters currents (e) the active and reactive current jnjected to the grid.

RSC and GSC rating power can be calculated as 412 and 457 kVA, respectively. However, this is much lower for the proposed configurations. The size of the dc-link capacitor is in a 1.5 MW conventional DFIG is about 16-21 mF [40-43]. In the proposed configuration, by choosing the bandwidth of the dc link voltage regulator 1/10 of that of the speed regulator, which is 10 Hz, and allowing 5% voltage variation the size of the capacitor should be larger than 16.6F.

To evaluate the proposed configuration in the case of a low voltage or fault, a low voltage ride through analysis has been conducted. The machine is protected using an active crowbar [44, 45] , pitch angle control [46]. The results are shown in Fig. 12. In Fig. 12 (a) the voltage at the Point of Common Coupling (PCC) drops to 15% at t=3 s and lasts for 0.625 seconds. The voltage at the stator terminal is slightly higher owing to the injection of reactive current during the fault. Active and reactive power of the generator before the fault is one and zero respectively. During the fault the active power drops to a small value as shown in Fig. 12 (b). Additionally, during the fault the proposed configuration injects reactive power and current as shown in Fig. 12 (b) and (e). The speed of the generator is controlled to remains close to synchronous speed and the speed of the turbine increases owing to the store of surplus power that cannot be transferred to the grid (Fig. 12 (c)). The current of the converter (Fig. 12 (d)) is limited to its nominal value by the active crowbar strategy and the dc-link voltage (Fig. 12 (a)) is controlled.

VI. Conclusion

This paper introduces a new structure for hydraulic WECS that eliminated the need for the GSC. The system uses a supercapacitor and only one converter, RSC, to supply the power to the rotor. This new structure controls the DC-link voltage by controlling the speed of the generator. Elimination of the GSC, its filter, and transformer (if any) reduces the overall cost of the system and increases the efficiency and reliability of the system. Furthermore, controlling the speed around the synchronous speed provides the opportunity to limit the rotor voltage and enables the utilization of a supercapacitor. The proposed configuration is capable of controlling the active and reactive power of the system with the need of only one converter RSC with a power rating of 2.7%. Compared to a conventional induction generator, the proposed configuration is capable of injecting reactive power into the grid.

References

[1] W. Vision, "A new era for wind power in the United States, US Department of Energy, 2015," ed: DOE/GO-102015-4557. Available from: https://www. energy. gov/eere/wind/maps …, 2017.

[2] D. Gielen, F. Boshell, D. Saygin, M. D. Bazilian, N. Wagner, and R. Gorini, "The role of renewable energy in the global energy transformation," *Energy Strategy Reviews*, vol. 24, pp. 38-50, 2019, doi: 10.1016/j.esr.2019.01.006.

[3] B. P. Center, "Annual Energy Outlook 2020," 2020.

[4] I. IRENA, "Renewable power generation costs in 2017," *Report, International Renewable Energy Agency, Abu Dhabi*, 2018.

[5] S. Sheng, "Report on wind turbine subsystem reliability-a survey of various databases (presentation)," National Renewable Energy Lab.(NREL), Golden, CO (United States), 2013.

[6] E. Artigao, S. Martín-Martínez, A. Honrubia-Escribano, and E. Gómez-Lázaro, "Wind turbine reliability: A comprehensive review towards effective condition monitoring development," *Applied energy*, vol. 228, pp. 1569-1583, 2018.

[7] J. Carroll, A. McDonald, and D. McMillan, "Failure rate, repair time and unscheduled O&M cost analysis of offshore wind turbines," *Wind Energy*, vol. 19, no. 6, pp. 1107-1119, 2016.

[8] N. Tazi, E. Châtelet, and Y. Bouzidi, "Using a hybrid cost-FMEA analysis for wind turbine reliability analysis," *Energies*, vol. 10, no. 3, p. 276, 2017.

[9] P. Asmus and M. Seitzler, "The wind energy operation & maintenance report," *Wind Energy Update*, 2010.

[10] A. Ragheb and M. Ragheb, "Wind turbine gearbox technologies," in *2010 1st international nuclear & renewable energy conference (INREC)*, 2010: IEEE, pp. 1-8.

[11] T. J. Stehly and P. C. Beiter, "2018 Cost of Wind Energy Review," National Renewable Energy Lab.(NREL), Golden, CO (United States), 2020.

[12] H. Polinder, F. F. Van der Pijl, G.-J. De Vilder, and P. J. Tavner, "Comparison of direct-drive and geared generator concepts for wind turbines," *IEEE Transactions on energy conversion*, vol. 21, no. 3, pp. 725-733, 2006.

[13] R. Poore and T. Lettenmaier, "Alternative Design Study Report: WindPACT Advanced Wind Turbine Drive Train Designs Study; November 1, 2000--February 28, 2002," National Renewable Energy Lab.(NREL), Golden, CO (United States), 2003.

[14] C. Qin, E. Innes-Wimsatt, and E. Loth, "Hydraulic-electric hybrid wind turbines: Tower mass saving and energy storage capacity," *Renewable Energy*, vol. 99, pp. 69-79, 2016, doi: 10.1016/j.renene.2016.06.037.

[15] M. Roggenburg *et al.*, "Techno-economic analysis of a hydraulic transmission for floating offshore wind turbines," *Renewable Energy*, vol. 153, pp. 1194-1204, 2020, doi: 10.1016/j.renene.2020.02.060.

[16] J. Schmitz, M. Vukovic, and H. Murrenhoff, "Hydrostatic Transmission for Wind Turbines: An Old Concept, New Dynamics," presented at the ASME/BATH 2013 Symposium on Fluid Power and Motion Control, 2013.

[17] M. Deldar, A. Izadian, and S. Anwar, "A decentralized multivariable controller for hydrostatic wind turbine drivetrain," *Asian Journal of Control*, vol. 22, no. 3, pp. 1038-1051, 2019, doi: 10.1002/asjc.2019.

[18] M. Deldar, A. Izadian, and S. Anwar, "Reconfiguration of a wind turbine with hydrostatic drivetrain to improve annual energy production," in *2015 IEEE Energy Conversion Congress and Exposition (ECCE)*, 2015: IEEE, pp. 6660-6666.

[19] A. Jarquin Laguna, "Steady-State Performance of the Delft Offshore Turbine," 2010.

[20] D. Rajabhandharaks and P. Hsu, "Optimal aerodynamic energy capture strategies for hydrostatic transmission wind turbine," in *2014 IEEE Conference on Technologies for Sustainability (SusTech)*, 2014: IEEE, pp. 140-147.

[21] B. Dolan and H. Aschemann, "Control of a wind turbine with a hydrostatic transmission—An extended linearisation approach," in *2012 17th International Conference on Methods & Models in Automation & Robotics (MMAR)*, 2012: IEEE, pp. 445-450.

[22] A. J. Laguna, J. W. van Wingerden, and N. F. B. Diepeveen, "Analysis of dynamics of fluid power drive-trains for variable speed wind turbines: parameter study," *IET Renewable Power Generation*, vol. 8, no. 4, pp. 398-410, 2014, doi: 10.1049/iet-rpg.2013.0134.

[23] H. T. Do, T. D. Dang, H. V. A. Truong, and K. K. Ahn, "Maximum Power Point Tracking and Output Power Control on Pressure Coupling Wind Energy Conversion System," *IEEE Transactions on Industrial Electronics*, vol. 65, no. 2, pp. 1316-1324, 2018, doi: 10.1109/tie.2017.2733424.

[24] M. Chen, S. M. Santos, and A. Izadian, "Torque-assisting compressed air energy storage hydraulic wind drivetrains," in *2016 IEEE Power and Energy Conference at Illinois (PECI)*, 2016: IEEE, pp. 1-5.

[25] L. Wei, Z. Liu, Y. Zhao, G. Wang, and Y. Tao, "Modeling and Control of a 600 kW Closed Hydraulic Wind Turbine with an Energy Storage System," *Applied Sciences*, vol. 8, no. 8, 2018, doi: 10.3390/app8081314.

[26] M. Vaezi and A. Izadian, "Energy storage techniques for hydraulic wind power systems," in *2014 International Conference on Renewable Energy Research and Application (ICRERA)*, 2014: IEEE, pp. 897-901.

[27] M. Saadat, F. A. Shirazi, and P. Y. Li, "Modeling and control of an open accumulator Compressed Air Energy Storage (CAES) system for wind turbines," *Applied Energy*, vol. 137, pp. 603-616, 2015.

[28] P. Y. Li, E. Loth, T. W. Simon, J. D. Van de Ven, and S. E. Crane, "Compressed air energy storage for offshore wind turbines," *Proc. International Fluid Power Exhibition (IFPE)*, 2011.

[29] Z. Liu, Y. Tao, L. Wei, P. Zhan, and D. Yue, "Analysis of Dynamic Characteristics of a 600 kW Storage Type Wind Turbine with Hybrid Hydraulic Transmission," *Processes*, vol. 7, no. 7, p. 397, 2019.

[30] C. Ai *et al.*, "Research on Quasi-Synchronous Grid-Connected Control of Hydraulic Wind Turbine," *IEEE Access*, vol. 8, pp. 126092-126108, 2020, doi: 10.1109/access.2020.3005136.

[31] J. B. Ekanayake, L. Holdsworth, X. Wu, and N. Jenkins, "Dynamic modeling of doubly fed induction generator wind turbines," *IEEE transactions on power systems*, vol. 18, no. 2, pp. 803-809, 2003.

[32] Y. Lei, A. Mullane, G. Lightbody, and R. Yacamini, "Modeling of the wind turbine with a doubly fed induction generator for grid integration studies," *IEEE transactions on energy conversion*, vol. 21, no. 1, pp. 257-264, 2006.

[33] B. Wu, Y. Lang, N. Zargari, and S. Kouro, *Power conversion and control of wind energy systems*. John Wiley & Sons, 2011.

[34] D. Aguglia, J. Cros, P. Viarouge, and R. Wamkeue, *Optimal selection of drive components for doubly-fed induction generator based wind turbines*. INTECH Open Access Publisher, 2011.

[35] Z. Chen, J. M. Guerrero, and F. Blaabjerg, "A review of the state of the art of power electronics for wind turbines," *IEEE Transactions on power electronics*, vol. 24, no. 8, pp. 1859-1875, 2009.

[36] E. Taherian-Fard, R. Sahebi, T. Niknam, A. Izadian, and M. Shasadeghi, "Wind Turbine Drivetrain Technologies," *IEEE Transactions on Industry Applications*, vol. 56, no. 2, pp. 1729-1741, 2020, doi: 10.1109/tia.2020.2966169.

[37] D. Rajabhandharaks, "Control of hydrostatic transmission wind turbine," 2014.

[38] M. Deldar, "Decentralized multivariable modeling and control of wind turbine with hydrostatic drive-train," Purdue University, 2016.

[39] R. Akbari, A. Izadian, and R. Weissbach, "An Approach in Torque Control of Hydraulic Wind Turbine Powertrains," in *2019 IEEE Energy Conversion Congress and Exposition (ECCE)*, 2019: IEEE, pp. 979-982.

[40] H. Nian, Y. Xu, L. Chen, and M. Zhu, "Modeling and analysis of dc-link dynamics in DFIG system with an indicator function," *IEEE Access*, vol. 7, pp. 125401-125412, 2019.

[41] J. Hu, Y. Huang, D. Wang, H. Yuan, and X. Yuan, "Modeling of grid-connected DFIG-based wind turbines for DC-link voltage stability analysis," *IEEE Transactions on Sustainable Energy*, vol. 6, no. 4, pp. 1325-1336, 2015.

[42] C. Liu, D. Xu, N. Zhu, F. Blaabjerg, and M. Chen, "DC-voltage fluctuation elimination through a DC-capacitor current control for DFIG converters under unbalanced grid voltage conditions," *IEEE Transactions on Power Electronics*, vol. 28, no. 7, pp. 3206-3218, 2012.

[43] D. Zhou and F. Blaabjerg, "Bandwidth oriented proportional-integral controller design for back-to-back power converters in DFIG wind turbine system," *IET Renewable Power Generation*, vol. 11, no. 7, pp. 941-951, 2017.

[44] G. Pannell, D. J. Atkinson, and B. Zahawi, "Minimum-threshold crowbar for a fault-ride-through grid-code-compliant DFIG wind turbine," *IEEE Transactions on Energy Conversion*, vol. 25, no. 3, pp. 750-759, 2010.

[45] O. Gomis-Bellmunt, A. Junyent-Ferre, A. Sumper, and J. Bergas-Jane, "Ride-through control of a doubly fed induction generator under unbalanced voltage sags," *IEEE Transactions on Energy Conversion*, vol. 23, no. 4, pp. 1036-1045, 2008.

[46] C. Ai, G. Zhou, Y. Wang, W. Gao, and X. Kong, "Active Power Control of Hydraulic Wind Turbines during Low Voltage Ride-Through (LVRT) Based on Hierarchical Control," *Energies*, vol. 12, no. 7, p. 1224, 2019.